Molecular Pharmacology Fast Forward. Published on July 6, 2018 as DOI: 10.1124/mol.118.112557
This article has not been copyedited and formatted. The final version may differ from this version.

Title: The zinc transporter SLC39A7 (ZIP7) is essential for regulation of cytosolic zinc levels

Authors: Grace Woodruff, Christian G. Bouwkamp, Femke M. de Vrij, Timothy Lovenberg, Pascal Bonaventure, Steven A. Kushner, Anthony W. Harrington

Affiliations:

Neuroscience Discovery, Janssen Research and Development, LLC, 3210 Merryfield Row, San Diego, CA 92121 (G.W., T.L., P.B., A.W.H.)

Department of Psychiatry, Erasmus MC, Wytemaweg 80, Rotterdam, The Netherlands (C.G.B., F.M.d.V., S.A.K.)

Molecular Pharmacology Fast Forward. Published on July 6, 2018 as DOI: 10.1124/mol.118.112557
This article has not been copyedited and formatted. The final version may differ from this version.

Running Title: ZIP7 Maintains Cytosolic Zinc Levels

Corresponding Author: Anthony W. Harrington, PhD. Neuroscience Discovery, Janssen Research and Development, LLC, 3210 Merryfield Row, San Diego, CA 92121. Phone: +1 858-320-3465. Email: aharrin1@its.jnj.com

Number of Text Pages: 24

Number of Tables: 0

Number of Figures: 7

Number of References: 27

Words in Abstract: 153

Words in Introduction: 546

Words in Discussion: 671

Abbreviations:

CHOP: CCAAT-Enhancer-Binding Protein Homologous Protein

CNVs: Copy Number Variations

ER: Endoplasmic Reticulum

GFP: Green Fluorescent Protein

ICP-MS: Inductively Coupled Plasma Mass Spectrometry

KO: Knock-out

PDI: Protein Disulfide Isomerase

SNPs: Single-Nucleotide Polymorphisms

WT: Wild-type

Molecular Pharmacology Fast Forward. Published on July 6, 2018 as DOI: 10.1124/mol.118.112557
This article has not been copyedited and formatted. The final version may differ from this version.

Abstract

Zinc homeostasis is a highly regulated process in mammalian cells that is critical for normal growth and development. Movement of zinc across cell compartments is controlled by two classes of transporters: Slc39a family members transport zinc into the cytosol from either the extracellular space or from intracellular stores such as the endoplasmic reticulum (ER), while the SSLC30A family mediates zinc efflux from the cytosol. Here we report that genetic ablation of SLC39A7 (ZIP7) results in decreased cytosolic zinc levels, increased ER zinc levels, impaired cell proliferation, and induction of ER stress. Confirmatory of impaired zinc transport as the causal mechanism, both the increased ER stress and impaired cell proliferation were rescued by increasing cytosolic zinc. Furthermore, using these robust cellular phenotypes we implemented a small molecule library screen with 2,800 compounds and identified one small molecule capable of rescuing ER stress and cell proliferation in ZIP7 deficient cells in the low micromolar range.

Molecular Pharmacology Fast Forward. Published on July 6, 2018 as DOI: 10.1124/mol.118.112557
This article has not been copyedited and formatted. The final version may differ from this version.

Introduction

Zinc is an essential metal that is required for normal growth and development in all higher plants and animals. Acting as a cofactor for over 2,000 proteins, zinc can modulate enzymatic activity and gene transcription (Hogstrand et al., 2009), as well as function as a second messenger in signaling pathways (Yamasaki et al., 2007). Since zinc cannot freely permeate lipid bilayers, active transport is required to move zinc across cellular and organelle membranes. There are two families of zinc transporters, categorized by their direction of zinc movement. The Solute Carrier family 30A (SLC30A), also known as the Zn transporter (ZnT) family, has 10 members that mobilize zinc from the cytosol. The Solute Carrier family 39A (SLC39A) family, also known as the Zrt-, Irt-related protein (ZIP) family, has 14 members that transport zinc into the cytosol from the extracellular space or from intracellular stores, such as the ER and Golgi. In addition to zinc, some members of the ZIP family also transport iron (Pinilla-Tenas et al., 2011), manganese (Girijashanker et al., 2008), and cadmium (Fujishiro et al., 2012).

Recent publications have identified the importance of ZnT and ZIP transporters in human health and disease. Mutations in SLC39A8 cause intellectual disability with cortical atrophy (Boycott et al., 2015), mutations in SLC39A14 (ZIP14) cause childhood-onset parkinsonism-dystonia (Tuschl et al., 2016) and mutations in SLC39A13 (ZIP13) cause a form of Ehlers-Danlos syndrome (Giunta et al., 2008). Additionally, single-nucleotide polymorphisms (SNPs) and copy number variations (CNVs) in other ZNT and ZIP family members have been associated with Bipolar Disorder (Baum et al., 2008), Schizophrenia (Carrera et al., 2012), Autism (Gazzellone et al., 2014; O'Roak et al., 2011), and other disorders (Kambe et al., 2015). Thus, elucidating the function of individual zinc transporters may help us understand the pathophysiology, treatment and prevention of zinc-related disease conditions.

ZIP7 is the only known ZIP family member that is localized to the ER membrane and is hypothesized to be responsible for mobilizing zinc from the ER, a zinc storage site, into the cytosol (Taylor et al., 2004). ZIP7 is critical for normal growth and development as the *ZIP7* knock-out

Molecular Pharmacology Fast Forward. Published on July 6, 2018 as DOI: 10.1124/mol.118.112557
This article has not been copyedited and formatted. The final version may differ from this version.

(KO) is embryonic lethal in mice, while loss-of-function mutations of the drosophila *ZIP7* homolog Catecholamines up (*Catsup*) lead to abnormal wing development (Groth et al., 2013). Furthermore, morpholino knockdown of *ZIP7* expression in zebrafish causes neurodevelopmental impairments, which can be rescued with zinc supplementation (Yan et al., 2012). At the cellular level, recent studies have illuminated a role for ZIP7 in the normal function of the ER and shown that loss of ZIP7 results in ER stress (Bin et al., 2017; Ohashi et al., 2016). However, the precise mechanism of how loss of ZIP7 causes ER stress and affects zinc levels has not been fully elucidated. Here we report that CRISPR-mediated genetic ablation of *ZIP7* in human cells results in severely decreased levels of cytosolic zinc, impaired cell proliferation, and activation of ER stress. Moreover, we demonstrate the causality of the impaired cytosolic zinc levels by fully rescuing both the impairment of cell proliferation and activation of ER stress by restoring cytosolic zinc levels. Finally, we implemented a small molecule screen based on the ER stress phenotype that yielded a lead compound with efficacy in fully rescuing the effects of *ZIP7* KO through a zinc-independent mechanism.

Materials and Methods

Cell Culture and Genome Editing

MG-63 cells were grown in EMEM supplemented with 10% FBS,1 X Pen/Strep, 1X NEAA and 1X Glutamine. Cells were split with trypsin every 3-4 days. MG-63 cells were transfected with Lipofectamine 3000 (ThermoFisher) and SpCas9 plasmid with sgRNA sequence: GCCACACTCACGAGAGCATCTGG. This sgRNA sequence targets exon 1 of SLC39A7. Seventy-two hours after transfection, GFP positive cells were sorted and plated at a density of 5000 cells per 10cm dish, such that single colonies could be isolated. Clones were manually picked when colonies were ~100 cells. Colonies were expanded and screened for ZIP7 KO based on disruption of DNA sequence and confirmed as knockout by western blot. Cell lines were

Molecular Pharmacology Fast Forward. Published on July 6, 2018 as DOI: 10.1124/mol.118.112557
This article has not been copyedited and formatted. The final version may differ from this version.

routinely checked to be free of mycoplasma infection using Lonza MycoAlert Mycoplasma Detection Kit (Lonza LT07).

Western Blot

Cells were lysed using RIPA buffer (ThermoFisher) with protease (Sigma) and phosphatase (Pierce) inhibitors. After centrifugation at 13,000*g*, protein concentration was measured using the BCA protein assay kit (Pierce) and lysates were separated on a 4–12% Bis-Tris gels (Invitrogen) using MES sodium dodecyl sulfate running buffer (Invitrogen). Proteins were transferred with the iBlot system onto nitrocellulose membranes (Novex). Membranes were blocked with 5% milk (Sigma) and then incubated with primary antibodies overnight at 4 degrees. Primary antibodies used: SLC39A7 anti-rabbit (1:500, Abcam 117560), and GAPDH anti-mouse (1:1000, Millipore 374). Blots were visualized using ECL western blotting detection reagents (Pierce).

Immunocytochemistry and Image Analysis

In each experiment, cells were plated at a density of 1,500 per well in 384 well Cell Carrier Ultra microplates (PerkinElmer). Cells were fixed with 4% paraformaldehyde at room temperature for 15 minutes followed by 3 washes with PBS. Cells were blocked in blocking buffer (5% BSA (Sigma) with 0.1% Triton-X (Sigma) in PBS) for 1 hour at room temperature followed by primary antibody incubation in blocking buffer overnight at 4 degrees. Cells were washed 3 times with PBS and then incubated with secondary antibodies for 1 hour at room temperature diluted in blocking buffer. Cells were washed 3 times with PBS and then imaged on a PerkinElmer Opera Phenix. Primary antibodies used: PDI anti-mouse (1:1000, Abcam 2792), PDI anti-rabbit (1:1000, Cell Signaling C81H6), SLC39A7 anti-rabbit (1:500, Abcam 117560), CHOP anti-mouse (1:3000, Cell Signaling L63F7). HCS CellMask Deep Red Stain (ThermoFisher) was used during the secondary antibody incubation at 1:10,000 to identify the entire cell. To stain nuclei, NucBlue (ThermoFisher) was used during the secondary antibody incubation per the manufacturer

Molecular Pharmacology Fast Forward. Published on July 6, 2018 as DOI: 10.1124/mol.118.112557
This article has not been copyedited and formatted. The final version may differ from this version.

instructions. Secondary antibodies used: Goat anti-rabbit Alexa Flour 488, Goat anti-mouse Alexa Flour 488, Goat anti-rabbit Alexa Flour 568 all from ThermoFisher were used at 1:500. In every experiment, 5 images per well were captured at 20x magnification and each experiment was performed in triplicate and was repeated a minimum of 3 times. Images were analyzed using Harmony Image Analysis System (PerkinElmer). Please see the supplemental data for more detail on image analysis. GraphPad Prism version 7 was used to perform all statistical analysis. All statistical tests were unpaired.

Phenotypic Screen

ZIP7$^{-/-}$ cells were plated at a density of 1,500 cells per well into 384 well Cell Carrier Ultra microplates (PerkinElmer). Twenty-four hours after plating, cells were treated with 1μM of compound. Pyrithione was used as the positive control at 500nM. Cells were fixed with 4% paraformaldehyde 48 hours after compound treatment. In the primary screen, cells were stained with CHOP and HCS CellMask Deep Red Stain as described above, and the CHOP nucleus/cytoplasm ratio was calculated using Columbus Image Analysis system. Hits were selected based on % inhibition of CHOP. Pyrithione was set as 100% inhibition and hits were determined based on 70% inhibition or above. In the secondary screen, the 33 hits from the primary screen were retested at 1μM in triplicate for 48 hours. In the secondary screen, cells were stained with CHOP, HCS Cell Mask and PDI as described above. Of the 33 primary hits, 30 of them confirmed to inhibit CHOP in the secondary screen. One compound (Compound A) was identified to not only inhibit CHOP, but also increased cell number and reduced PDI intensity and area.

Synthesis of Compound A

The synthesis of Compound A is described in U.S. Patent US2008/080081 in example 24 (Illig et al., 2016).

Molecular Pharmacology Fast Forward. Published on July 6, 2018 as DOI: 10.1124/mol.118.112557
This article has not been copyedited and formatted. The final version may differ from this version.

Zinc Quantification by ICP-MS

Cells were plated in 10cm dishes and were harvested 72 hours after plating. Dishes were treated with either vehicle (H_2O) or 500nM Pyrithione. Equal number of cells were fractionated to cytosol and ER fractions by first collecting cells and spinning down at 300 x g. Supernatant was removed and cells were resuspended in sucrose buffer (0.32M sucrose + 10mM HEPES). Cells were homogenized by syringe-based homogenization. Next, homogenized cells were spun at 300 x g for 10 minutes to remove nuclei. Supernatant from homogenized cells was then centrifuged at 100,000 x g for 1 hour. The supernatant was removed and analyzed as the cytosolic fraction. The pellet was resuspended in sucrose buffer and analyzed as the microsome fraction which contains the ER. Zinc concentrations in the cytosol and microsome fraction were determined by inductively coupled plasma mass spectrometry (ICP-MS). Iridium was used as the internal standard. Samples or standards were combined with the internal standard, digested in 1% nitric acid, then infused into the ICP-MS for quantitation. Zinc concentrations were normalized to the total number of cells.

RNA-seq and q-PCR

Total RNA from 3 biological replicates per genotype was extracted using the Qiagen RNeasy Mini Kit according to the manufacturer's instructions. RNA-seq and analysis was performed by Novogene (Beijing, China). Briefly, libraries were constructed using NEBNext UltraTM RNA Library Prep Kit following manufacturer's instructions and PCR products were purified using AMPure XP System (Beckman Coulter). The library quality was assessed on the Agilent Bioanlyzer 2100 system. The library was sequenced on an Illumina Hiseq platform. On average, 65.8 million reads were obtained per sample. Raw reads were processed through Novogene in-house scripts to obtain clean reads, by removing reads containing adapters, reads containing poly-N and low-quality reads. On average, 53 million clean reads were obtained per sample.

Molecular Pharmacology Fast Forward. Published on July 6, 2018 as DOI: 10.1124/mol.118.112557
This article has not been copyedited and formatted. The final version may differ from this version.

Reads were aligned to the reference genome using TopHat v2.0.12., 89.84% of reads were uniquely mapped. FPKM (fragments per kilobase of transcript per million mapped reads) of each gene was calculated based on the length of the gene and reads mapped to each gene. Differential gene expression analysis was performed using DESeq2 R package. The p values were adjusted using the Benjamini and Hochberg's method. Genes with an adjusted p value <0.05 were considered as differentially expressed. GO enrichment analysis was performed using GOseq, based on Wallenius non-central hyper-geometric distribution.

For q-PCR, total RNA was extracted as described above. RNA was reverse-transcribed into cDNA using Superscript III reverse transcriptase (Invitrogen) with random hexamer primers. Transcript abundance was determined by quantitative PCR using SYBR Green PCR mix (Applied Biosystems). Transcripts were normalized to GAPDH and each sample was run in triplicate with 3 biological samples per genotype. SLC39A8 (ZIP8) Forward: GGCCCCTTCAAACAGGTACA, Reverse: TGCTGTCACAGAAGCTAATGG SLC39A14 (ZIP14) Forward: GCAGCTTCATGGTGACTGAA, Reverse: GCTAAGCTGCTTCTGCCG SLC30A1 (ZNT1) Forward: TCACCACTTCTGGGGTTTTC, Reverse: ACCAGGAGGAGACCAACACC SLC30A5 (ZNT5) Forward: TTTGAAGGCTGTGGGACTTTTCG, Reverse: GGTGTTTGGTAATAGTTTTCCCAG GAPDH Forward: AGGTCGGTGTGAACGGATTTG, Reverse: TGTAGACCATGTAGTTGAGGTCA

Results

Generation and RNAseq analysis of ZIP7 KO cells

To elucidate the role of ZIP7 in human cells, we utilized CRISPR genome editing (Shalem et al., 2014) to genetically ablate *ZIP7* from the osteosarcoma cell line, MG-63. MG-63 cells are large cells that are ideal for imaging and amendable to transfection and viral transduction. We identified 2 clones out of 18 screened that had indels in the first exon that introduce premature stop codons. *ZIP7* mRNA was significantly decreased in *ZIP7*$^{-/-}$ cells, consistent with nonsense

Molecular Pharmacology Fast Forward. Published on July 6, 2018 as DOI: 10.1124/mol.118.112557
This article has not been copyedited and formatted. The final version may differ from this version.

mediated decay. Moreover, ZIP7 protein was undetectable by western blot in *ZIP7*$^{-/-}$ clones (Figure 1B). We next used *ZIP7*$^{+/+}$ and *ZIP7*$^{-/-}$ cells to confirm the localization of ZIP7 to the ER as has previously been reported (Bin et al., 2017; Taylor et al., 2004). Immunocytochemical labeling of ZIP7$^{+/+}$ cells with antibodies to the ER specific enzyme Protein Disulfide Isomerase (PDI) and ZIP7 confirmed strong colocalization of ZIP7 with PDI, validating the localization of ZIP7 to the ER (Figure 1A). Importantly, ZIP7 staining was absent other than minimal background labeling in ZIP7$^{-/-}$ cells, thereby confirming the specificity of the ZIP7 antibody.

To investigate the function of ZIP7 in human cells, we performed RNA-sequencing (RNA-seq) on *ZIP7*$^{+/+}$ and *ZIP7*$^{-/-}$ cells. There were 6055 differentially expressed genes between *ZIP7*$^{+/+}$ and *ZIP7*$^{-/-}$ cells with an adjusted p value of <0.05 (Figure 1C), including upregulation of four zinc transporters. The transporters *ZIP8*, *ZIP14*, *ZNT1* and *ZNT5* all had a two-fold or greater upregulation in *ZIP7*$^{-/-}$ vs. *ZIP7*$^{+/+}$ cells when measured by quantitative-PCR analysis (q-PCR) (Figure 1D). To further identify cellular processes that were altered by deletion of *ZIP7*, we performed Gene Ontology (GO) analysis. GO analysis revealed two significantly enriched categories: 1) protein processing in the endoplasmic reticulum, and 2) cell cycle (Figure 1E). These results are consistent with a recent report that *ZIP7* knockdown induces ER stress genes and downregulates genes involved in the cell cycle (Bin et al., 2017).

Loss of ZIP7 Causes Decreased Cell Proliferation and ER Stress

To establish the RNA-seq hypothesized functional consequences of *ZIP7* KO, we first examined cell proliferation. We plated equal numbers of *ZIP7*$^{+/+}$ and *ZIP7*$^{-/-}$ cells, and quantified the number of nuclei at 24, 48, and 72 hours. *ZIP7*$^{+/+}$ cells more than doubled in number during the 72-hour period, whereas the number of *ZIP7*$^{-/-}$ cells did not significantly increase (Figure 2A). We next examined whether *ZIP7*$^{-/-}$ cells exhibit ER stress as predicted by the RNA-seq data by comparing the staining intensity of the ER marker PDI in *ZIP7*$^{+/+}$ and *ZIP7*$^{-/-}$ cells (Figure 2C). Indeed, *ZIP7*$^{-/-}$ cells exhibited significantly increased intensity of PDI (Figure 2B), consistent with

Molecular Pharmacology Fast Forward. Published on July 6, 2018 as DOI: 10.1124/mol.118.112557
This article has not been copyedited and formatted. The final version may differ from this version.

ER stress (Ko et al., 2002). Moreover, in addition to the increase of PDI intensity, we also observed a parallel increase of the area of PDI staining in *ZIP7*$^{-/-}$ cells. Specifically, we quantified the area of PDI staining as a proportion of the cytoplasmic area which confirmed a significant expansion of the PDI-labeled ER in *ZIP7*$^{-/-}$ cells (Figure 2D), again consistent with ER stress. In order to further evaluate this possibility, we also examined the localization of CHOP, a transcription factor that is localized to the cytoplasm under normal conditions, but translocates to the nucleus under conditions of ER stress (Ron and Habener, 1992). Consistent with ER stress, *ZIP7*$^{-/-}$ cells exhibited strong nuclear localization of CHOP in contrast to *ZIP7*$^{+/+}$ cells (Figure 2E, F). Taken together, based on the increased intensity of PDI labeling, expansion of PDI-labeled ER area, and nuclear localization of CHOP, there is substantial evidence to suggest that *ZIP7*$^{-/-}$ cells have increased ER stress.

WT ZIP7 Rescues Proliferation and ER Stress Phenotypes

To confirm that both the cell proliferation and ER stress phenotypes are dependent on ZIP7, we infected cells with lentivirus to overexpress either GFP, WT ZIP7, or a previously reported loss-of-function ZIP7^{G178D} mutant (Groth et al., 2013). Overexpression of WT ZIP7 in *ZIP7*$^{-/-}$ cells rescued cell proliferation, compared to transduction with GFP or ZIP7^{G178D} (Figure 3A and B). WT ZIP7 expression also rescued ER stress, with a decrease in the CHOP nucleus/cytoplasmic ratio, PDI intensity and PDI area (Figure 3C, D, and E) compared to GFP or ZIP7^{G178D} transduced cells (Figure 3C, D, and E). These results conclusively demonstrate that loss of ZIP7 results in decreased cell proliferation and induction of ER stress.

ZIP7 is Essential for Regulation of Cytosolic Zinc Levels

The ER is a site of zinc storage and it has been hypothesized that ZIP7 transports zinc into the cytoplasm from the ER stores (Taylor et al., 2008). However, whether loss of ZIP7 affects ER or cytosolic zinc levels has never been conclusively demonstrated. Given our confirmation of

Molecular Pharmacology Fast Forward. Published on July 6, 2018 as DOI: 10.1124/mol.118.112557
This article has not been copyedited and formatted. The final version may differ from this version.

earlier studies demonstrating that ZIP7 is localized to the ER (Figure 1), we sought to measure zinc concentrations in the ER and cytosol using subcellular fractionation of *ZIP7*$^{+/+}$ and *ZIP7*$^{-/-}$ cells. Specifically, we measured zinc concentrations in the respective ER and cytosolic fractions using inductively coupled plasma mass spectrometry (ICP-MS). Consistent with previous reports in wild-type cells (Qin et al., 2011; Sun et al., 2015), we observed that the zinc concentration in the cytoplasmic fraction (~1400ng/mL) was significantly higher than zinc levels in the ER fraction (~500ng/mL) (Figure 4A, B). In contrast, *ZIP7*$^{-/-}$ cells exhibited a significant increase of ER zinc concentration and decrease of cytosolic zinc concentration (Figure 4A, B). These results are consistent with a model whereby ZIP7 transports zinc from the ER into the cytosol, for which loss of ZIP7 results in a shift of the equilibrium towards an increased ER zinc concentration. Therefore, to directly test this hypothesis, we treated cells with pyrithione, an ionophore that transports zinc through the cell membrane. Indeed, when *ZIP7*$^{-/-}$ cells were treated with 500nM pyrithione, cytosolic zinc levels were significantly increased compared to vehicle, nearly reaching the concentration observed in *ZIP7*$^{+/+}$ cells (Figure 4A, B). This was presumably due to pyrithione's ability to shuttle the free zinc present in fetal bovine serum (a component of the media) into the cells. We did not observe any changes in ER zinc in these cells, confirming that the increased ER zinc concentration in *ZIP7*$^{-/-}$ cells results from an inability to transport zinc out of the ER, rather than a cytoplasmic impairment due to the increased concentration of cytosolic zinc (Figure 4A, B). Therefore, ZIP7 is essential for maintaining both ER and cytosolic zinc levels.

Cell Proliferation and ER Stress are Rescued by Restoring Cytosolic Zinc

Given our observation that treating ZIP7$^{-/-}$ cells with pyrithione can largely restore cytosolic zinc levels, we next asked whether this was sufficient to rescue the cell proliferation and ER stress phenotypes. Importantly, given that pyrithione rescued the abnormal cytosolic, but not ER, concentration of zinc in *ZIP7*$^{-/-}$ cells (Figure 4), this also provided us the opportunity to gauge whether the cell proliferation and ER stress phenotypes are driven by cytoplasmic or ER zinc

Molecular Pharmacology Fast Forward. Published on July 6, 2018 as DOI: 10.1124/mol.118.112557
This article has not been copyedited and formatted. The final version may differ from this version.

concentrations. *ZIP7*$^{-/-}$ cells were treated with pyrithione for 72 hours followed by quantification of nuclei density, PDI intensity, PDI area and CHOP nuclear/cytoplasmic ratio. Treatment with pyrithione induced significantly increased proliferation within 72 hours (Figure 5B). Moreover, pyrthione treatment also resulted in significantly decreased PDI intensity, PDI area and nuclear localization of CHOP (Figure 5A, C, D, E, F). Together, these findings establish the causality of decreased cytosolic zinc levels in mediating the impaired cell proliferation and induction of ER stress in *ZIP7*$^{-/-}$ cells.

Phenotypic Drug Screen in ZIP7$^{-/-}$ *Cells*

Phenotypic drug screening is a powerful tool to identify compounds that affect a given cellular phenotype. Such screening functions in a target-agnostic manner and has the possibility of uncovering novel biology. We performed a small-scale drug screen with 2816 internal kinase inhibitor compounds at a concentration of 1μM to search for compounds that alleviate ER stress in *ZIP*$^{-/-}$ cells using the nuclear translocation of CHOP as a readout. We used pyrithione treatment as a positive control and selected compounds with at least 70% inhibition of CHOP translocation compared to the positive control. Based on these criteria, we identified 33 compound hits. To confirm the hits, we performed a secondary screen in triplicate in which we also quantified cell number, PDI intensity and PDI area. Of the 33 initial hits, 30 were confirmed to inhibit CHOP translocation when tested in triplicate. Interestingly, we identified 1 compound (Compound A) that significantly inhibited CHOP translocation, increased cell number, and decreased PDI intensity and area (Figure 6D, E, F and G). We tested Compound A in dose response and only found an effect at 1μM (Supplemental Figure 1). The structure of Compound A (4-Cyano-N-[2-(4,4-dimethylcyclohex-1-en-1-yl)-4-(2,2,6,6-tetramethyl-1,1-dioxidotetrahydro-2H-thiopyran-4-yl)phenyl]-1H-imidazole-2-carboxamide) is shown in Figure 6C. Compound A was identified internally as an inhibitor of CSF1R with an IC50 of ~3nM (data not shown). However, Compound A is not rescuing the ZIP7$^{-/-}$ phenotypes in a CSF1R-dependent manner because ZIP7$^{-/-}$ cells do

Molecular Pharmacology Fast Forward. Published on July 6, 2018 as DOI: 10.1124/mol.118.112557
This article has not been copyedited and formatted. The final version may differ from this version.

not express CSF1R (data not shown). Additionally, other CSF1R inhibitors were present in the screening library but did not rescue the ZIP7$^{-/-}$ phenotypes (data not shown). We also tested Compound A in *ZIP7*$^{+/+}$ cells and observed that Compound A does not have any effect on proliferation or ER stress in *ZIP7*$^{+/+}$ cells (Supplemental Figure 2). This result demonstrates that Compound A is specific for rescuing phenotypes associated with loss of ZIP7. To test whether Compound A is an inhibitor of other kinases, we performed the Eurofins kinase selectivity panel (1 μM) and found that Compound A inhibits many other kinases. However, of those kinases, ZIP7$^{-/-}$ cells only express JAK1, PDK1, PLK4, STK16 and TYK2 (Supplemental Table 1). When we tested whether commercially available inhibitors of those kinases could rescue ZIP7$^{-/-}$ phenotypes, none had any significant impact on cell number, CHOP translocation, PDI intensity, or PDI area. Thus, Compound A is rescuing ZIP7$^{-/-}$ phenotypes through a mechanism other than CSF1R, JAK1, PDK1, PLK4, STK16 or TYK2 inhibition.

Lastly, to examine whether the mechanism of action by which Compound A rescued the cellular phenotypes was zinc-dependent, we treated *ZIP7*$^{-/-}$ cells with Compound A and measured cellular zinc levels by ICP-MS. We found no significant differences in cytosolic or ER zinc concentrations when cells were treated with Compound A (Figure 6H and I). This result demonstrates that ER stress and proliferation caused by *ZIP7* ablation can be rescued by zinc-independent mechanisms. We also tested whether Compound A could block ER stress induced by Tunicamycin, Brefeldin A or Thapsigargin. We treated *ZIP7*$^{+/+}$ cells with Compound A and found no significant differences in the CHOP nucleus/cytoplasmic ratio (Figure 7C). Treating *ZIP7*$^{+/+}$ cells with Tunicamycin, Brefeldin A and Thapsigargin induced CHOP translocation to the nucleus (Figure 7C). Interestingly, Compound A failed to block CHOP translocation induced by Tunicamycin, Brefeldin A or Thapsigargin (Figure 7C). These results demonstrate that Compound A may be specific for rescuing ER stress only when ER stress is induced by low cytosolic zinc.

Discussion

Molecular Pharmacology Fast Forward. Published on July 6, 2018 as DOI: 10.1124/mol.118.112557
This article has not been copyedited and formatted. The final version may differ from this version.

In this study, we investigated the role of ZIP7 in the regulation of cellular zinc levels. We found that CRISPR/Cas9-mediated ablation of *ZIP7* results in significantly decreased zinc concentration in the cytosol and increased zinc levels in the ER, with concomitant abnormalities in cell proliferation and ER stress. Both phenotypes are rescued when *ZIP7* is overexpressed or when cytosolic zinc levels are restored with pyrithione. Additionally, we identified a small-molecule that completely rescues the phenotypic effects of ZIP7 KO by a zinc-independent mechanism, which might have important implications for treating diseases of aberrant zinc homeostasis.

Zinc has a well-established role as a frequent cofactor in enzyme catalysis and protein folding (Andreini and Bertini, 2012; Andreini et al., 2011). More recently, zinc also has a proposed role as a second messenger for intracellular signaling and transduction pathways. Thus, establishing how cytosolic zinc levels are regulated is important for understanding how cells maintain a variety of critical functions. In this study, we definitively demonstrate that ZIP7 is essential for maintenance of cytosolic zinc levels. Even though we observed upregulation of other zinc transporters in *ZIP7*$^{-/-}$ cells, these changes were not sufficient to compensate for the loss of ZIP7. This suggests that ZIP7 is obligatory for maintaining cytosolic zinc. Furthermore, we show that insufficient zinc levels in the cytosol impairs cell proliferation and induces ER stress. Treatment of *ZIP7*$^{-/-}$ cells with pyrithione rescued ER stress phenotypes, but notably only with restoration of cytosolic zinc levels and without any evidence of a restored ER zinc concentration. Previous studies hypothesized that accumulation of zinc in the ER was the cause of ER stress in ZIP7 deficiency (Bin et al., 2017), but based on the selective rescue of cytosolic, but not ER, zinc by pyrithione, our findings indicate that low cytosolic zinc was the driver of both ER stress and proliferation defects. Bin et al hypothesized that elevated zinc in the ER causes PDI to aggregate, which prevents the proper folding of proteins and ultimately leads to ER stress(Bin et al., 2017). Therefore, although our results demonstrate that low levels of zinc in the cytosol are the cause of ER stress, we cannot rule out that altered activity of PDI might also be a contributing factor.

Molecular Pharmacology Fast Forward. Published on July 6, 2018 as DOI: 10.1124/mol.118.112557
This article has not been copyedited and formatted. The final version may differ from this version.

ZIP7 is one of the 10% of genes that are consistently upregulated in breast cancer (Hogstrand et al., 2009). Our results suggest that increased expression of ZIP7 could cause growth advantages, possibly by increasing zinc levels in the cytosol. Thus, targeting intracellular zinc levels could be of therapeutic benefit in breast cancer. One way to modulate intracellular zinc would be to identify modulators of ZIP transporters that reside on the cell surface. Our results suggest that intracellular zinc levels need to be carefully fine-tuned as low intracellular zinc causes growth retardation, for which increased cytosolic zinc may lead to a growth advantage.

To date there are numerous reports of mutations in ZnT and ZIP transporters that cause disease and dozens of SNPs that may contribute to an array of medical conditions. Presumably these mutations are causing aberrant zinc or other metal homeostasis, which highlights the need for therapies that can compensate for changes in zinc transporter activity or function, however this remains to be systemically evaluated. In our study, we identified a compound that completely rescues the proliferation and ER stress consequences of ZIP7 KO, which validates that disorders of zinc homeostasis can be therapeutically targeted. Moreover, given that the compound that we identified rescues ER stress and proliferation without changing zinc levels, phenotypes caused by aberrant metal homeostasis appear to be possible to rescue by zinc-independent mechanisms. Future studies to elucidate both the zinc-dependent and zinc-independent mechanisms hold therapeutic potential for treating disease caused by zinc imbalances.

In conclusion, we propose that ZIP7 is an essential regulator of cytosolic zinc levels and that sufficient levels of zinc in the cytosol are necessary for normal proliferation and normal ER function. ZIP7 could be a therapeutic target for conditions in which zinc levels are dysregulated or in conditions of high ER stress.

Acknowledgments

The authors thank Kristopher Standish for support with RNA-seq analysis.

Molecular Pharmacology Fast Forward. Published on July 6, 2018 as DOI: 10.1124/mol.118.112557
This article has not been copyedited and formatted. The final version may differ from this version.

Authorship Contributions

Participated in Research Design: Woodruff, Buowkamp, de Vrij, Lovenberg, Bonaventure, Kushner, Harrington.

Conducted Experiments: Woodruff

Performed Data Analysis: Woodruff

Wrote or Contributed to Writing of the Manuscript: Woodruff, Bonaventure, Kushner, Harrington.

References

Molecular Pharmacology Fast Forward. Published on July 6, 2018 as DOI: 10.1124/mol.118.112557
This article has not been copyedited and formatted. The final version may differ from this version.

Andreini, C., and Bertini, I. (2012). A bioinformatics view of zinc enzymes. Journal of Inorganic Biochemistry *111*, 150-156.

Andreini, C., Bertini, I., and Cavallaro, G. (2011). Minimal Functional Sites Allow a Classification of Zinc Sites in Proteins. PloS one *6*, e26325.

Baum, A.E., Hamshere, M., Green, E., Cichon, S., Rietschel, M., Noethen, M.M., Craddock, N., and McMahon, F.J. (2008). Meta-analysis of two genome-wide association studies of bipolar disorder reveals important points of agreement. Molecular psychiatry *13*, 466-467.

Bin, B.H., Bhin, J., Seo, J., Kim, S.Y., Lee, E., Park, K., Choi, D.H., Takagishi, T., Hara, T., Hwang, D.*, et al.* (2017). Requirement of Zinc Transporter SLC39A7/ZIP7 for Dermal Development to Fine-Tune Endoplasmic Reticulum Function by Regulating Protein Disulfide Isomerase. The Journal of investigative dermatology *137*, 1682-1691.

Boycott, K.M., Beaulieu, C.L., Kernohan, K.D., Gebril, O.H., Mhanni, A., Chudley, A.E., Redl, D., Qin, W., Hampson, S., Kury, S.*, et al.* (2015). Autosomal-Recessive Intellectual Disability with Cerebellar Atrophy Syndrome Caused by Mutation of the Manganese and Zinc Transporter Gene SLC39A8. Am J Hum Genet *97*, 886-893.

Carrera, N., Arrojo, M., Sanjuán, J., Ramos-Ríos, R., Paz, E., Suárez-Rama, J.J., Páramo, M., Agra, S., Brenlla, J., Martínez, S.*, et al.* (2012). Association Study of Nonsynonymous Single Nucleotide Polymorphisms in Schizophrenia. Biological Psychiatry *71*, 169-177.

Fujishiro, H., Yano, Y., Takada, Y., Tanihara, M., and Himeno, S. (2012). Roles of ZIP8, ZIP14, and DMT1 in transport of cadmium and manganese in mouse kidney proximal tubule cells. Metallomics *4*, 700-708.

Gazzellone, M.J., Zhou, X., Lionel, A.C., Uddin, M., Thiruvahindrapuram, B., Liang, S., Sun, C., Wang, J., Zou, M., Tammimies, K.*, et al.* (2014). Copy number variation in Han Chinese individuals with autism spectrum disorder. Journal of Neurodevelopmental Disorders *6*, 34.

Girijashanker, K., He, L., Soleimani, M., Reed, J.M., Li, H., Liu, Z., Wang, B., Dalton, T.P., and Nebert, D.W. (2008). Slc39a14 gene encodes ZIP14, a metal/bicarbonate symporter: similarities to the ZIP8 transporter. Molecular pharmacology *73*, 1413-1423.

Giunta, C., Elçioglu, N.H., Albrecht, B., Eich, G., Chambaz, C., Janecke, A.R., Yeowell, H., Weis, M., Eyre, D.R., Kraenzlin, M.*, et al.* (2008). Spondylocheiro Dysplastic Form of the Ehlers-Danlos Syndrome—An Autosomal-Recessive Entity Caused by Mutations in the Zinc Transporter Gene SLC39A13. The American Journal of Human Genetics *82*, 1290-1305.

Groth, C., Sasamura, T., Khanna, M.R., Whitley, M., and Fortini, M.E. (2013). Protein trafficking abnormalities in Drosophila tissues with impaired activity of the ZIP7 zinc transporter Catsup. Development *140*, 3018-3027.

Hogstrand, C., Kille, P., Nicholson, R.I., and Taylor, K.M. (2009). Zinc transporters and cancer: a potential role for ZIP7 as a hub for tyrosine kinase activation. Trends in molecular medicine *15*, 101-111.

Illig, C.R., Chen, J., Meegalla, S.K., and Wall, M.J. (2016). Inhibitors of c-fms kinase (Google Patents).

Kambe, T., Tsuji, T., Hashimoto, A., and Itsumura, N. (2015). The Physiological, Biochemical, and Molecular Roles of Zinc Transporters in Zinc Homeostasis and Metabolism. Physiological reviews *95*, 749-784.

Ko, H.S., Uehara, T., and Nomura, Y. (2002). Role of ubiquilin associated with protein-disulfide isomerase in the endoplasmic reticulum in stress-induced apoptotic cell death. The Journal of biological chemistry *277*, 35386-35392.

O'Roak, B.J., Deriziotis, P., Lee, C., Vives, L., Schwartz, J.J., Girirajan, S., Karakoc, E., Mackenzie, A.P., Ng, S.B., Baker, C.*, et al.* (2011). Exome sequencing in sporadic autism spectrum disorders identifies severe de novo mutations. Nature genetics *43*, 585-589.

Ohashi, W., Kimura, S., Iwanaga, T., Furusawa, Y., Irie, T., Izumi, H., Watanabe, T., Hijikata, A., Hara, T., Ohara, O.*, et al.* (2016). Zinc Transporter SLC39A7/ZIP7 Promotes Intestinal Epithelial Self-Renewal by Resolving ER Stress. PLoS genetics *12*, e1006349.

Pinilla-Tenas, J.J., Sparkman, B.K., Shawki, A., Illing, A.C., Mitchell, C.J., Zhao, N., Liuzzi, J.P., Cousins, R.J., Knutson, M.D., and Mackenzie, B. (2011). Zip14 is a complex broad-scope metal-ion transporter whose functional properties support roles in the cellular uptake of zinc and nontransferrin-bound iron. American Journal of Physiology-Cell Physiology *301*, C862-C871.

Qin, Y., Dittmer, P.J., Park, J.G., Jansen, K.B., and Palmer, A.E. (2011). Measuring steady-state and dynamic endoplasmic reticulum and Golgi Zn2+ with genetically encoded sensors. Proceedings of the National Academy of Sciences *108*, 7351-7356.

Ron, D., and Habener, J.F. (1992). CHOP, a novel developmentally regulated nuclear protein that dimerizes with transcription factors C/EBP and LAP and functions as a dominant-negative inhibitor of gene transcription. Genes & development *6*, 439-453.

Shalem, O., Sanjana, N.E., Hartenian, E., Shi, X., Scott, D.A., Mikkelsen, T.S., Heckl, D., Ebert, B.L., Root, D.E., Doench, J.G.*, et al.* (2014). Genome-Scale CRISPR-Cas9 Knockout Screening in Human Cells. Science *343*, 84-87.

Sun, Q., Zhong, W., Zhang, W., Li, Q., Sun, X., Tan, X., Sun, X., Dong, D., and Zhou, Z. (2015). Zinc deficiency mediates alcohol-induced apoptotic cell death in the liver of rats through activating ER and mitochondrial cell death pathways. American Journal of Physiology-Gastrointestinal and Liver Physiology *308*, G757-G766.

Taylor, K.M., Morgan, H.E., Johnson, A., and Nicholson, R.I. (2004). Structure-function analysis of HKE4, a member of the new LIV-1 subfamily of zinc transporters. The Biochemical journal *377*, 131-139.

Taylor, K.M., Vichova, P., Jordan, N., Hiscox, S., Hendley, R., and Nicholson, R.I. (2008). ZIP7-mediated intracellular zinc transport contributes to aberrant growth factor signaling in antihormone-resistant breast cancer Cells. Endocrinology *149*, 4912-4920.

Tuschl, K., Meyer, E., Valdivia, L.E., Zhao, N., Dadswell, C., Abdul-Sada, A., Hung, C.Y., Simpson, M.A., Chong, W.K., Jacques, T.S.*, et al.* (2016). Mutations in SLC39A14 disrupt manganese homeostasis and cause childhood-onset parkinsonism-dystonia. Nature communications *7*, 11601.

Yamasaki, S., Sakata-Sogawa, K., Hasegawa, A., Suzuki, T., Kabu, K., Sato, E., Kurosaki, T., Yamashita, S., Tokunaga, M., Nishida, K.*, et al.* (2007). Zinc is a novel intracellular second messenger. The Journal of Cell Biology *177*, 637-645.

Yan, G., Zhang, Y., Yu, J., Yu, Y., Zhang, F., Zhang, Z., Wu, A., Yan, X., Zhou, Y., and Wang, F. (2012). Slc39a7/zip7 plays a critical role in development and zinc homeostasis in zebrafish. In PloS one, pp. e42939.

Molecular Pharmacology Fast Forward. Published on July 6, 2018 as DOI: 10.1124/mol.118.112557
This article has not been copyedited and formatted. The final version may differ from this version.

Figure Legends

Figure 1. Generation and RNA-seq Analysis of *ZIP7*$^{-/-}$ Cells. A) Representative images of *ZIP7*$^{+/+}$ and *ZIP7*$^{-/-}$ cells stained with ZIP7 (green), PDI (red) and DAPI (blue). *ZIP7*$^{+/+}$ cells show colocalization of ZIP7 with PDI. *ZIP7*$^{-/-}$ cells exhibit minimal background staining with the ZIP7 antibody. B) Western blot of *ZIP7*$^{+/+}$ and *ZIP7*$^{-/-}$ cell lysates for ZIP7 and GAPDH expression. There is no detectable ZIP7 protein in *ZIP7*$^{-/-}$ clones. C) Histographs of differentially expressed genes in *ZIP7*$^{-/-}$ cells. D) Quantification of *ZIP8*, *ZIP14*, *ZNT1* and *ZNT5* in *ZIP7*$^{+/+}$ and *ZIP7*$^{-/-}$ cells. Error bars represent SEM (n=4). Significant differences between *ZIP7*$^{+/+}$ and *ZIP7*$^{-/-}$ were determined by Student's t-test (** $P < .01$). E) GO analysis of *ZIP7*$^{+/+}$ and *ZIP7*$^{-/-}$ cells. Protein processing in ER and cell cycle were the two significantly different pathways in *ZIP7*$^{+/+}$ compared to *ZIP7*$^{-/-}$.

Figure 2. *ZIP7* KO Causes Decreased Proliferation and Induction of ER Stress. A) Quantification of cell number in *ZIP7*$^{+/+}$ and *ZIP7*$^{-/-}$ cells after 24h, 48h and 72h. There are significantly less *ZIP7*$^{-/-}$ cells compared to *ZIP7*$^{+/+}$ cells, 48h and 72h after plating. B) Quantification of PDI intensity in *ZIP7*$^{+/+}$ and *ZIP7*$^{-/-}$ cells. There is a significant increase in PDI intensity in *ZIP7*$^{-/-}$ relative to *ZIP7*$^{+/+}$ cells. Values are expressed a fold change in intensity relative to *ZIP7*$^{+/+}$ cells. C) Representative images of *ZIP7*$^{+/+}$ and *ZIP7*$^{-/-}$ cells. PDI (green) and CellMask (red). D) Quantification of ER area in *ZIP7*$^{+/+}$ and *ZIP7*$^{-/-}$ cells. There is a significant increase in the ER area in *ZIP7*$^{-/-}$ cells compared to *ZIP7*$^{+/+}$ cells. E) Quantification of CHOP in the nucleus versus the cytoplasm in *ZIP7*$^{+/+}$ and *ZIP7*$^{-/-}$ cells. There is a significant increase in CHOP in the nucleus versus the cytoplasm in *ZIP7*$^{-/-}$ cells compared to *ZIP7*$^{+/+}$ cells. F) Representative images of *ZIP7*$^{+/+}$ and *ZIP7*$^{-/-}$ cells stained with CHOP (green). Error bars represent SEM from 3 independent experiments (n=3). Significant differences between *ZIP7*$^{+/+}$ and *ZIP7*$^{-/-}$ cells were determined by Student's t-test (**$P<0.01$).

Molecular Pharmacology Fast Forward. Published on July 6, 2018 as DOI: 10.1124/mol.118.112557
This article has not been copyedited and formatted. The final version may differ from this version.

Figure 3. Overexpression of WT *ZIP7* Rescues Cell Proliferation and ER Stress Phenotypes. A) Representative images of *ZIP7*$^{-/-}$ cells either untransduced or transduced with GFP, WT *ZIP7* or *ZIP7*^{G178D} for 72 hours and stained with PDI (orange). B) Quantification of cell number after 72 hours of transduction. WT ZIP7 significantly increased cell number compared to untransduced cells. There were no significant differences in *ZIP7* G178D transduced cells. C) Quantification of nuclear/cytoplasmic CHOP after 72 hours of transduction. Translocation of CHOP was significantly decreased in cells transduced with WT *ZIP7* compared to untransduced cells. D) Quantification of PDI intensity 72 hours after virus transduction. PDI intensity was significantly decreased in WT *ZIP7* transduced cells. E) Quantification of ER area. ER area was significantly decreased in WT *ZIP7* transduced cells. Error bars represent SEM from 3 independent experiments (n=3). Significant differences were determined by one-way ANOVA followed by Dunnett's test (**P<0.01).

Figure 4. ZIP7 KO Causes Reduced Zinc in the Cytoplasm and Increased Zinc in the ER. A) ER concentrations of zinc from *ZIP7*$^{+/+}$ and *ZIP7*$^{-/-}$ cells with vehicle and 500nM pyrithione treatment. *ZIP7*$^{-/-}$ cells exhibit significantly increased ER zinc levels compared to *ZIP7*$^{+/+}$ cells with vehicle treatment. ER zinc levels are not significantly changed with Pyrithione treatment. B) Cytosol concentrations of zinc from *ZIP7*$^{+/+}$ and *ZIP7*$^{-/-}$ cells with vehicle and 500nM pyrithione treatment. *ZIP7*$^{-/-}$ cells have significantly decreased cytosol zinc levels compared to *ZIP7*$^{+/+}$ cells. Error bars represent SEM (n=6). Significant differences between vehicle and pyrithione treated cells were determined by Student's t-test (** P < .01).

Figure 5. Pyrithione Treatment Rescues ER Stress and Proliferation in *ZIP7*$^{-/-}$ Cells. A) Representative images of *ZIP7*$^{-/-}$ cells treated with or vehicle pyrithione for 72 hours. Cells were stained with CHOP (green) and PDI (orange). B) Quantification of cell number in vehicle and pyrithione treated cells. C) Quantification of CHOP in the nucleus versus the cytoplasm in vehicle

Molecular Pharmacology Fast Forward. Published on July 6, 2018 as DOI: 10.1124/mol.118.112557
This article has not been copyedited and formatted. The final version may differ from this version.

and pyrithione treated cells. D) Quantification of PDI intensity in vehicle and pyrithione treated cells. Values are expressed as fold change relative to vehicle. E) Quantification of ER area in vehicle and pyrithione treated cells. Values are expressed as fold change relative to vehicle. In all graphs, error bars represent SEM from 3 independent experiments (n=3). Significant differences between vehicle and pyrithione treated cells were determined by Student's t-test (**P<0.01).

Figure 6. Phenotypic Screen for Small Molecules that Rescue ER Stress and Proliferation in *ZIP7*$^{-/-}$ Cells. A) Schematic of screening results. 2816 small molecules were screened at a concentration of 1μM. There were 33 primary hits that inhibit CHOP translocation to the nucleus and 30 of those were confirmed in the secondary screen. One compound was identified to rescue all ZIP7$^{-/-}$ phenotypes including cell number, PDI intensity and ER area. B) Representative images of vehicle and compounds that rescue CHOP nuclear translocation, PDI intensity and PDI area. Cells are stained with CHOP (green) and PDI (orange). C) Structures of Compound A. D) Quantification of cell number in vehicle and compound treated cells. E) Quantification of CHOP in the nucleus versus the cytosol. Values are expressed as relative to vehicle. F) Quantification of PDI intensity in vehicle and compound treated cells. Values are expressed as relative to vehicle. G) Quantification of ER area in vehicle and compound treated cells. Values are expressed as relative to vehicle. Error bars in all graphs represent SEM from 3 independent experiments (n=3). Significant differences between vehicle and compound treated cells were determined by Student's t-test (**P<0.01).

Figure 7. Compound A Rescues *ZIP7*$^{-/-}$ Phenotypes Independent of Zinc Levels. A) Quantification of cytosolic zinc concentration by ICP-MS. Compound A does not significantly alter cytosolic zinc levels. B) Quantification of ER zinc levels by ICP-MS. Compound A does not significantly alter ER zinc levels. Error bars represent SEM from 3 biological replicates. C) Quantification of CHOP

Molecular Pharmacology Fast Forward. Published on July 6, 2018 as DOI: 10.1124/mol.118.112557
This article has not been copyedited and formatted. The final version may differ from this version.

in the nucleus versus the cytosol in cells treated with inducers of ER stress. Tunicamycin, Brefeldin A and Thapsigargin induce CHOP translocation to the nucleus and Compound A does not block the CHOP translocation. Significant differences between vehicle and ER stress inducer were determined by one-way ANOVA followed by Dunnett's test (**P<0.01). There were no significant differences between ER stress inducer treated cells vs ER stress inducer and Compound A treated cells. Error bars represent SEM from 3 independent experiments (n=3).

Figure 1.

Molecular Pharmacology Fast Forward. Published on July 6, 2018 as DOI: 10.1124/mol.118.112557
This article has not been copyedited and formatted. The final version may differ from this version.

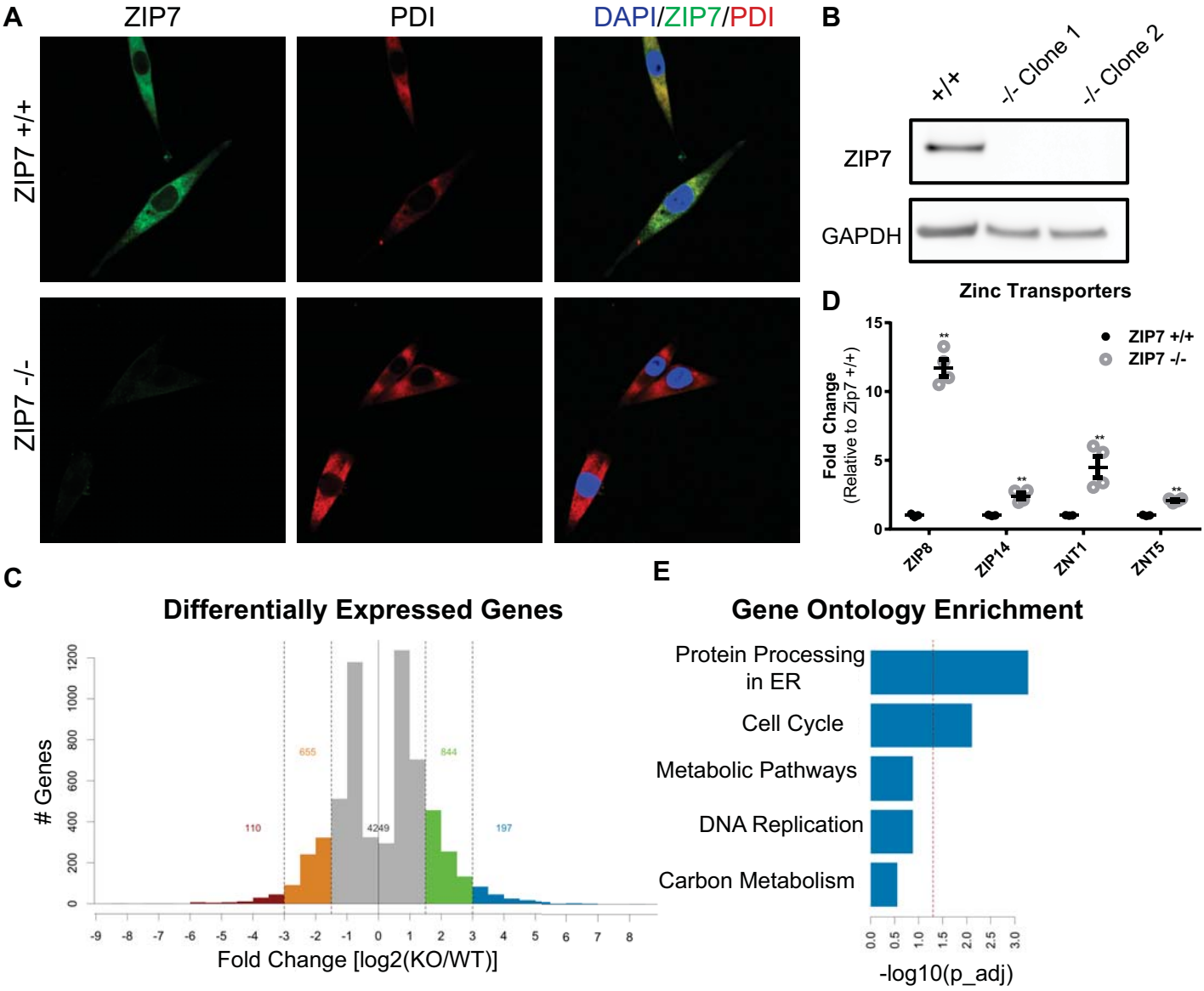

Figure 2.

Molecular Pharmacology Fast Forward. Published on July 6, 2018 as DOI: 10.1124/mol.118.112557
This article has not been copyedited and formatted. The final version may differ from this version.

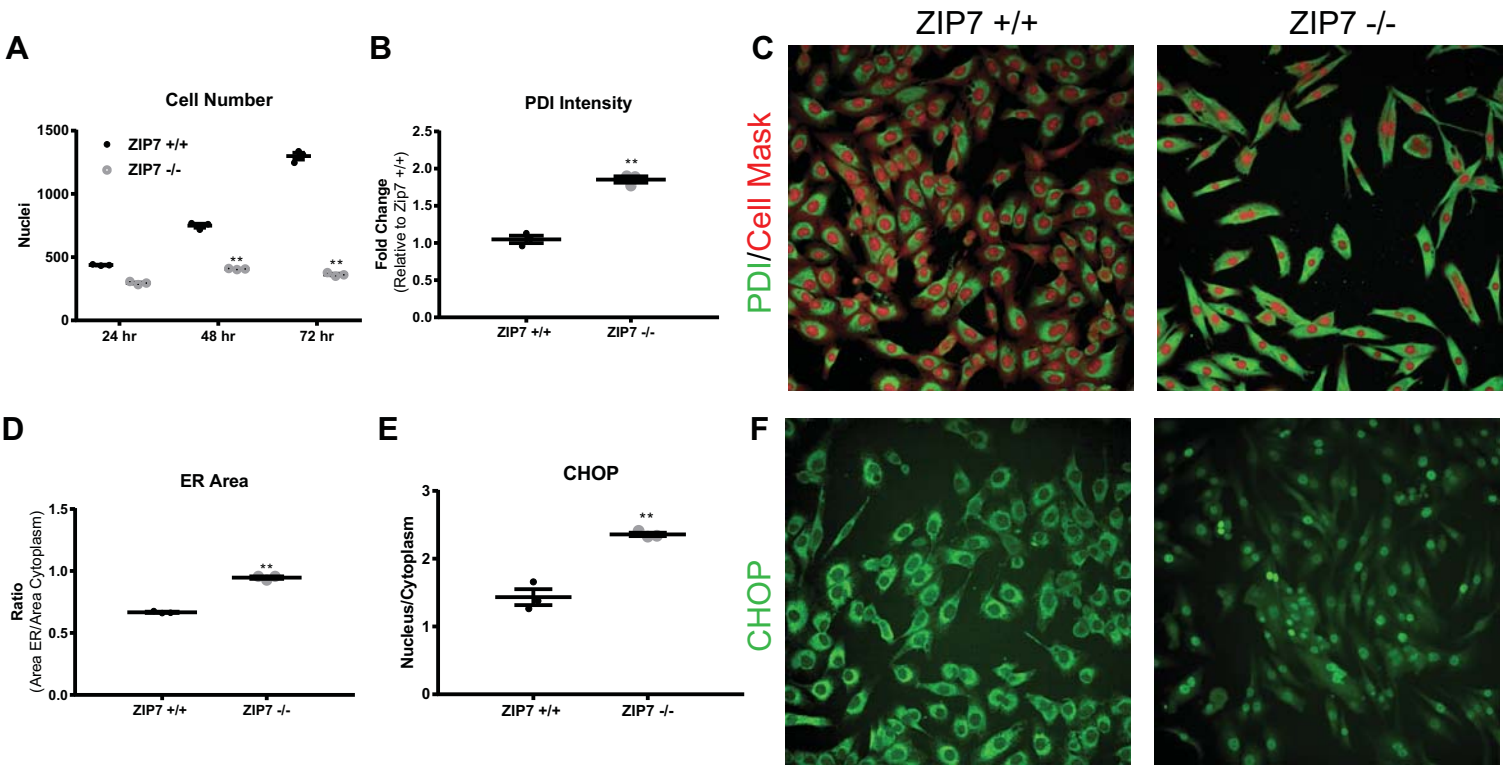

Molecular Pharmacology Fast Forward. Published on July 6, 2018 as DOI: 10.1124/mol.118.112557
This article has not been copyedited and formatted. The final version may differ from this version.

Figure 3.

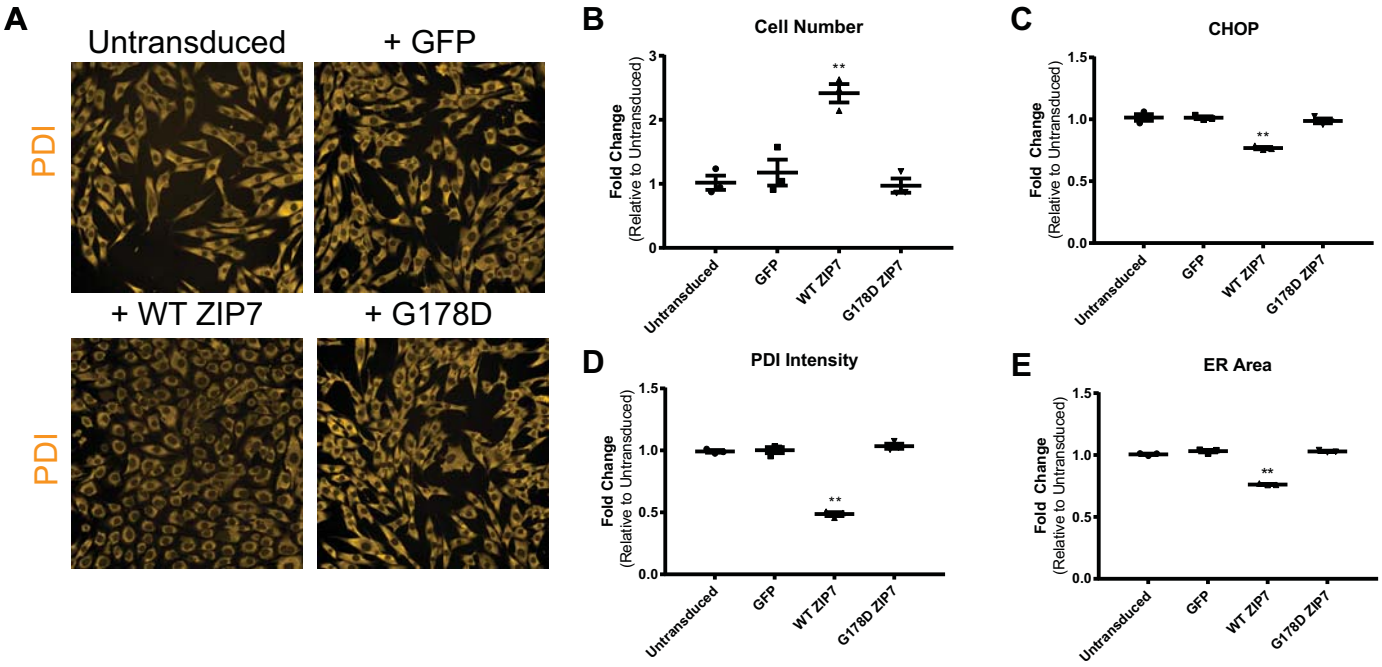

Molecular Pharmacology Fast Forward. Published on July 6, 2018 as DOI: 10.1124/mol.118.112557
This article has not been copyedited and formatted. The final version may differ from this version.

Figure 4.

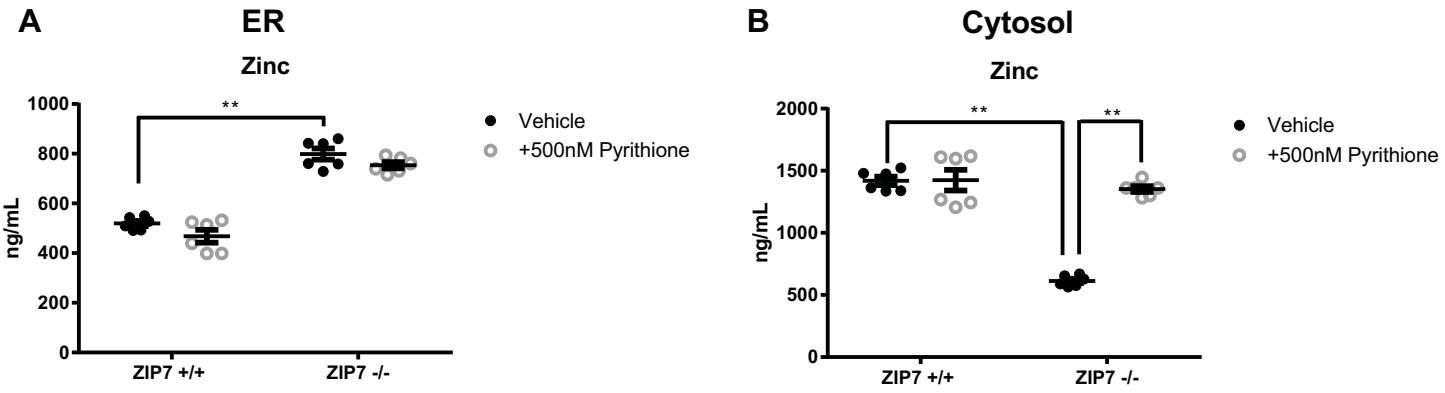

Figure 5.

Molecular Pharmacology Fast Forward. Published on July 6, 2018 as DOI: 10.1124/mol.118.112557
This article has not been copyedited and formatted. The final version may differ from this version.

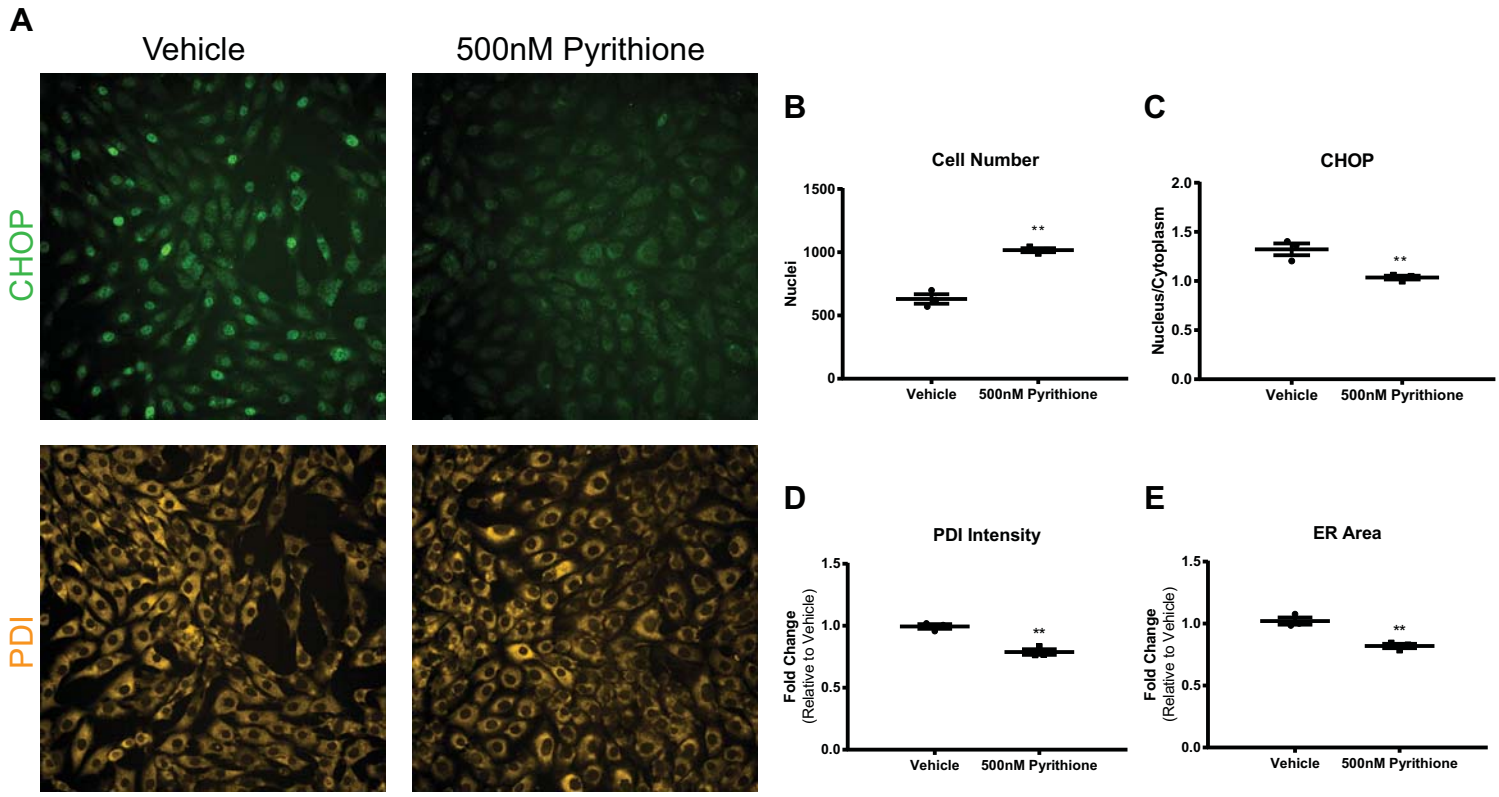

Molecular Pharmacology Fast Forward. Published on July 6, 2018 as DOI: 10.1124/mol.118.112557
This article has not been copyedited and formatted. The final version may differ from this version.

Figure 6.

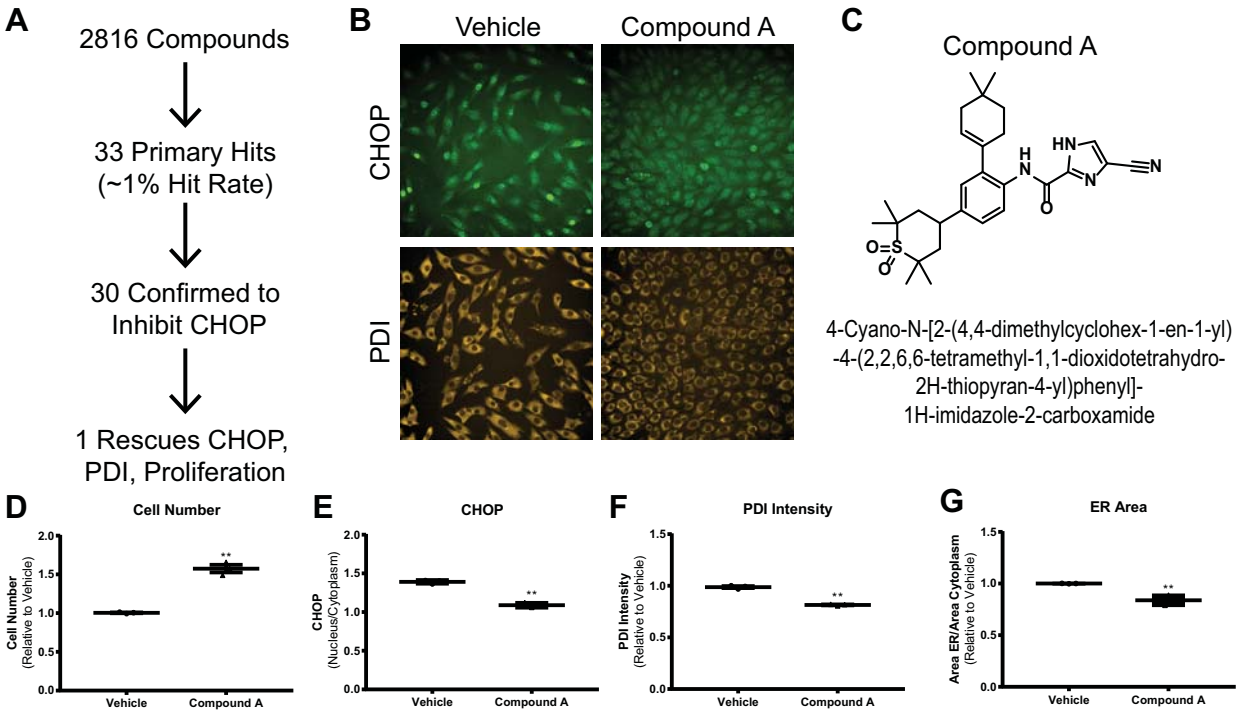

Molecular Pharmacology Fast Forward. Published on July 6, 2018 as DOI: 10.1124/mol.118.112557
This article has not been copyedited and formatted. The final version may differ from this version.

Figure 7.

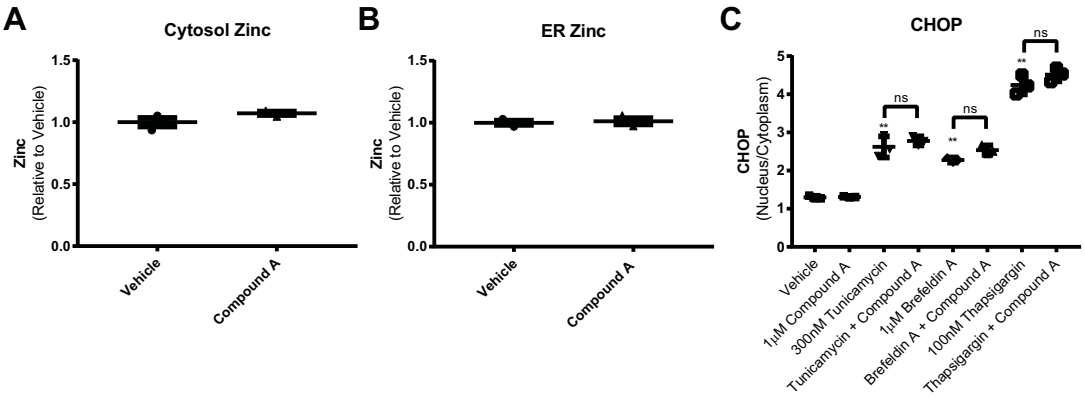

Supplemental Data

The zinc transporter SLC39A7 (ZIP7) is essential for regulation of cytosolic zinc

Authors: Grace Woodruff, Christian G. Bouwkamp, Femke M. de Vrij, Timothy Lovenberg, Pascal Bonaventure, Steven A. Kushner, Anthony W. Harrington

Molecular Pharmacology

Supplemental Table 1. Compound A Inhibits Multiple Kinases. Compound A was tested at 1μM in the Eurofins kinase selectivity panel. Compound A inhibited multiple kinases, but only JAK1, PDK1, PLK4, STK15 and TYK2 were expressed in ZIP7$^{-/-}$ cells. Values are percent activity of each kinase in the presence of 1μM Compound A. Commercially available inhibitors of JAK1, PDK1, PLK4, STK16, TYK2 were tested in ZIP7$^{-/-}$ cells and all failed to rescue ZIP7$^{-/-}$ phenotypes.

Kinase	Compound A @ 1μM	Expressed in ZIP7$^{-/-}$ Cells
JAK1	15	Yes
PDK1	66	Yes
PLK4	8	Yes
STK16	2	Yes
TYK2	4	Yes

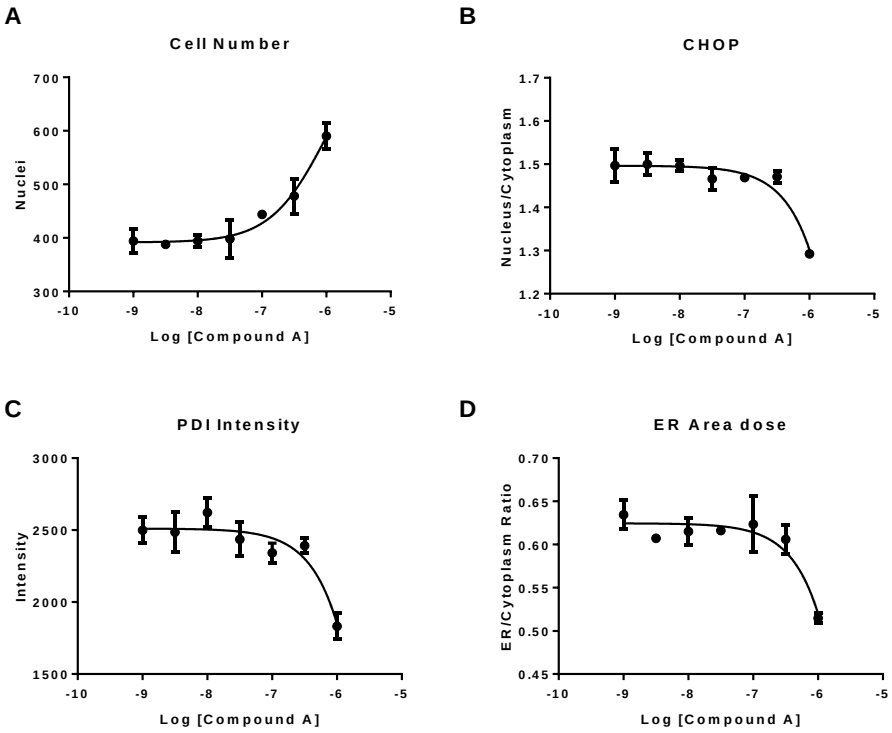

Supplemental Figure 1. Compound A dose response. A) Quantification of cell number in ZIP7$^{-/-}$ cells treated in dose response with Compound A. B) Quantification of the CHOP nucleus/cytoplasm ratio in ZIP7$^{-/-}$ cells treated in dose response with Compound A. C) Quantification of PDI intensity in ZIP7$^{-/-}$ cells treated in dose response with Compound A. D) Quantification of ER area in ZIP7$^{-/-}$ cells treated in dose response with Compound A. Compound A only showed an effect at 1μM.

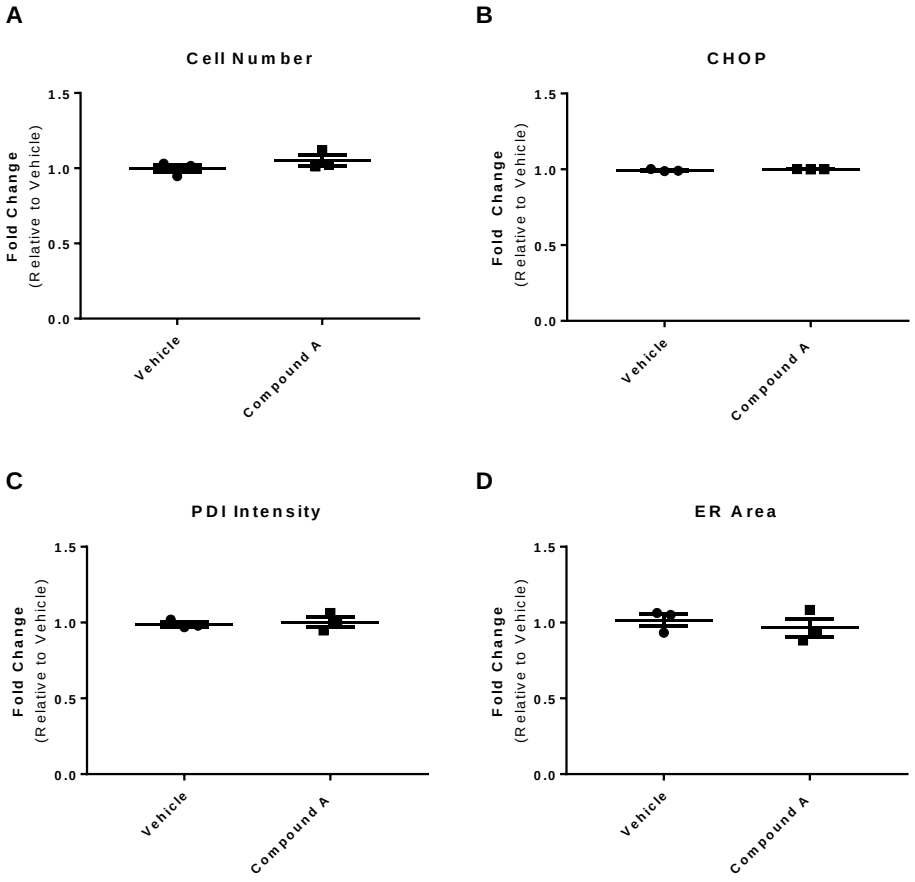

Supplemental Figure 2. Compound A has no effect on cell number, CHOP translocation, PDI intensity or ER area in ZIP7$^{+/+}$ cells. A) Quantification of cell number in ZIP7$^{+/+}$ cells treated with vehicle or 1μM Compound A. B) Quantification of CHOP nucleus/cytoplasm ratio in in ZIP7$^{+/+}$ cells treated with vehicle or 1μM Compound A. C) Quantification of PDI intensity in ZIP7$^{+/+}$ cells treated with vehicle or 1μM Compound A. D) Quantification of ER area in in ZIP7$^{+/+}$ cells treated with vehicle or 1μM Compound A. Error bars represent SEM of 3 biological replicates.

Supplemental Methods

Images were acquired on an Opera confocal microplate imaging system (PerkinElmer) with a 20x water objective. Five fields were acquired per well. Images were analyzed using Harmony Image Analysis Software (PerkinElmer). The parameters used to identify nuclei were DAPI channel: method B, common threshold 0.4, area > 30um2. The parameters used to identify the cytoplasm were: method A, individual threshold 0.15. Mean intensities in the cytoplasm or nucleus were calculated using the region of interest. Area of the cytoplasm was calculated based on the cytoplasm region of interest.

A **B** **C**

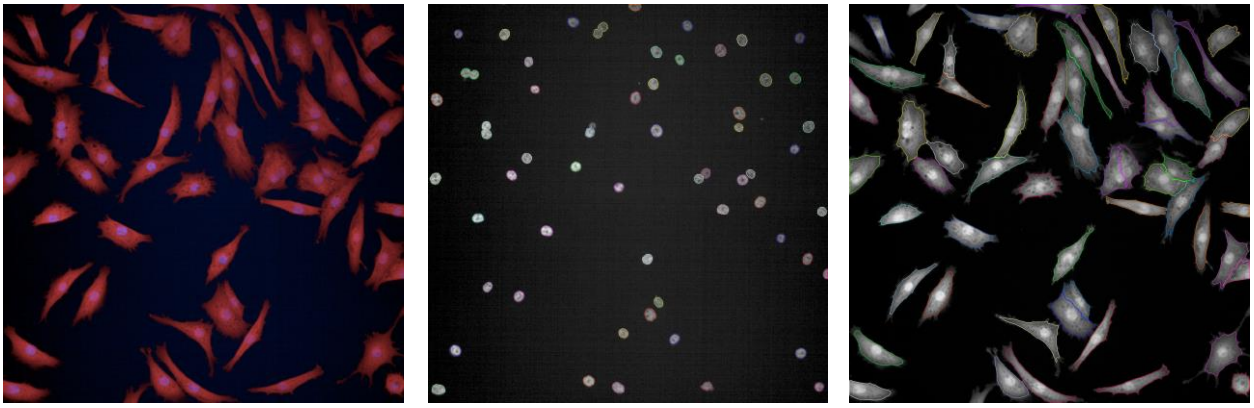

A) Example input image stained with DAPI (blue) and CellMask (red). B) Example image of nuclei identified using Harmony software. C) Example image of cytoplasm identified using Harmony software. Mean intensities per cell and areas were calculated based on the regions of interest identified in B and C. Each data point on the graphs in the manuscript represents the average of a minimum of 250 cells.